Korean J. Chem. Eng., 37(1), 80-92 (2020)
DOI: 10.1007/s11814-019-0424-6

pISSN: 0256-1115
eISSN: 1975-7220

Magnetic nanocomposite of filamentous algae activated carbon for efficient elimination of cephalexin from aqueous media

Shirin Afshin*,*, Yousef Rashtbari*,***, Bahman Ramavandi****,*****, Mehdi Fazlzadeh**,***, Mehdi Vosoughi**,***,†, Seyad Ahmad Mokhtari***, Mohammad Shirmardi******,*******,********, and Rabia Rehman*********

*Students Research Committee, School of Health, Ardabil University of Medical Sciences, Ardabil, Iran
**Social Determinants of Health Research Center, Ardabil University of Medical Sciences, Ardabil Iran
***Department of Environmental Health Engineering, School of Public Health, Ardabil University of Medical Sciences, Ardabil, Iran
****Systems Environmental Health and Energy Research Center, The Persian Gulf Biomedical Sciences Research Institute, Bushehr University of Medical Sciences, Bushehr, Iran
*****Department of Environmental Health Engineering, Faculty of Health and Nutrition, Bushehr University of Medical Sciences, Bushehr, Iran
******Social Determinants of Health Research Center, Health Research Institute, Babol University of Medical Sciences, Babol, Iran
*******Environmental Health Research Center, Health Research Institute, Babol University of Medical Sciences, Babol, Iran
********Department of Environmental Health Engineering, School of Public Health, Babol University of Medical Sciences, Babol, Iran
*********Institute of Chemistry, University of Punjab, New Campus, Lahore-54590, Pakistan
(*Received 19 June 2019 • accepted 8 November 2019*)

Abstract−Discharge of antibiotics into the environment can cause problems like increase of the microorganisms' resistance, disturbing the ecological balance and increasing the allergy in humans. In this research, an activated carbon was produced from filamentous algae and then magnetized with Fe_3O_4. The adsorbent size was nano-scale and its characteristics were studied using XRD, FT-IR, FE-SEM, BET and VSM techniques. The response surface method (RSM) was employed to optimize the operating parameters and determine the best conditions for cephalexin removal by novel composite of AC-Fe_3O_4. The various parameters in the process, such as reaction time, initial pH, adsorbent dose, initial concentration of cephalexin and effect of cations and anions that could interfere in the adsorption of cephalexin were evaluated in three levels. The proposed quadratic model was found to be best suggested model for the adsorption process (R^2=0.99094 and R^2_{adj}=0.9991). According to results, the parameters such as cephalexin concentration, the adsorbent dose, the reaction time and the pH value were found to be 28.16 mg/L, 2 g/L, 30.04 and 3.02, respectively. Experimental results showed that the adsorption of cephalexin followed Langmuir isotherm (R^2=0.9803). Also, the results showed cephalexin adsorption on the composite fitted pseudo-second-order kinetics. The study showed that the AC-Fe_3O_4 adsorbent has high efficacy for eliminating cephalexin from aqueous solution.

Keywords: Adsorption, Magnetic Activated Carbon, Cephalexin, Response Surface Methodology, Filamentous Algae

INTRODUCTION

The quality of available water resources has been changing due to the large volume of pollutants discharged into the receiving waters [1,2]. Discharge of toxic pollutants into the environment causes adverse effects on human health, agricultural products, and natural ecosystems [3]. Today, the public consumption of drugs has increased for various reasons, such as the spread of infectious diseases, the progress of medical sciences and pharmacy, and medical development [4]. Antibiotics are commonly employed for curing contagious diseases in humans and animals. Some of the antibiotics are used in agriculture to protect fruits against various infections. Iran is considered to be among the 20 top countries and second in Asia for drug consumption per capita. From the 1980s, several pieces of evidence on the presence of drugs residues in natural water resources have been reported [5]. The residues of antibiotics in the form of parent compounds or metabolites enter into water steams [6].

Approximately 30-90% of the antibiotics consumed by human beings and animals are not metabolized in the body and without any change excreted out into sewerage. Drugs found in drinking water include various types of analgesics, anti-seizure drugs, antimicrobials, lipid regulators, non-steroidal anti-inflammatory drugs and synthetic hormones [7]. The most important effects of antibiotics on the environment are the increased drug resistance of microorganisms, disturbance of environmental balance, and increased allergies in human beings. Cephalexin (CEX) is one of the cephalosporin families of beta-lactam species. This drug is one of the most used antibiotics for the treatment of respiratory and urinary tract infections. CEX is also widely used in veterinary medicine for treatment of mastitis and other infectious diseases. The resistance of bacteria to antibiotics has been reported in sewage, surface water, drinking water, farmland and aquaculture [8]. The decomposition

†To whom correspondence should be addressed.
E-mail: mvn_20@yahoo.com

of these compounds due to their complex structure and their low biodegradability is an important ecological challenge [9].

Various methods have been used to remove CEX from wastewater, such as membrane processes [10], advanced oxidation processes [11] and adsorption [12]. Some of the methods mentioned above for the removal of CEX are highly complex and costly due to the presence of a stable Naphthol ring (as the main structure) and the toxicity of antibiotics for microorganisms and their low biodegradability [13]. Advanced oxidation processes can change the polarity and functional groups in the pharmaceutical composition, which may be more harmful as compared to their primary compounds [14]. The cost of required chemicals and energy in advanced oxidation processes is a problem to use it on a practical or industrial scale [15]. In membrane processes, the operating costs and membrane construction are high [16].

The adsorption method is promising for the eradication of pharmaceutics from wastewater streams due to its high efficiency, low energy consumption, simplicity and low costs of the process. Activated carbon [17], zeolite [18], clay [19] and chitosan [20] have been examined for the removal of various pollutants including antibiotics. Activated carbon, in comparison to other adsorbents, is one of the most important adsorbents with regard to its high specific surface area, high adsorption capacity, more porous structure, and selective adsorption capability [21]. Along with the benefits mentioned for activated carbon, various studies reported several problems such as difficulty in the recovery and separation of activated carbon from the aqueous phase on an industrial scale [22]. Many studies have been carried out to overcome this problem, including the use of magnetic separation by iron oxide nanoparticles [23] and cobalt [24]. Iron oxide nanoparticles have gained much more interest due to their non-toxicity, rapid and simple separation process by an external magnetic field. Another advantage of using this kind of nano-material is overcoming the problem of filters' blocking [25]. However, their adsorption capacity is lower because of their surface structure [26].

Preparation of comercial activated carbon has high cost, so researchers are looking for low cost material for production of activated carbon. Filamentous algae are considered as agricultural wastes that grow in an agricultural stream. Farmers should remove this type of aqueous plant from the streams to facilitate passing of water to irrigation land. Filamentous algae have smooth and wooly structure, which makes it a promising raw matter for preparing activated carbon due to its availability. RSM, which is one of the effective methods for designing the experimental conditions, is a statistical technique based on the fit of a polynomial equation to the experimental data that must define the behavior of a data set with the objective of making statistical previsions. It can be well applied when a response or a set of responses of interest are influenced by several variables. The objective is to simultaneously optimize the levels of these variables to attain the best system performance [27]. Another benefit of this method is the ability to perform analysis of variance (Anova) to determine the final formula for pollutant removal and optimal theoretical conditions. The Box-Behnken method is a design based on three-dimensional factorial [28]. In this study, RSM using the Box-Behnken model design was used to find the optimized conditions and also to evaluate their effects on response function (CEX removal efficiency). The novelty of this study is preparing activated carbon from filamentous algae for first time with chemical activation method. In this study, activated carbon prepared from filamentous algae in combination with Fe_3O_4 nanoparticle (AC-Fe_3O_4 nanocomposite) was used as a new adsorbent for CEX removal from water streams.

Table 1. Chemical structural and main characteristics of CEX antibiotic

Chemical structure	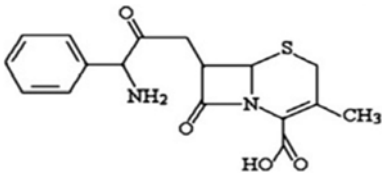
pKa1	2.56
pKa2	6.88
Molecular formula	$C_{16}H_{17}N_3O_4S$
(Molecular weight) (g/mol)	347.38
λ_{max}	261

MATERIALS AND METHODS

1. Materials and Solutions

This study was performed in a batch system. All materials used in this study were purchased from Merck in analytical grade. CEX was purchased from Sina Darou Co., Iran for preparing synthetic polluted samples. The general characteristics of CEX are presented in Table 1 [29]. Solutions of 0.1 M H_2SO_4 or NaOH were used for adjusting pH. The stock of CEX solution was made by mixing 1 g CEX powder in 1,000 mL of distilled water (1,000 ppm). Then, solutions with the required concentrations of CEX were prepared by diluting the stock solution.

2. Preparation of Activated Carbon from Filamentous Algae

The filamentous algae were collected from streams surrounding Ardabil city, Iran, then rinsed with distilled water to remove contaminants and impurities. The algae were then placed at room temperature for 12 hours and then in an oven at 70 °C for 12 hours. Finally, the algae were powdered by a convenient crusher (lab mill model: OML-1, Osaka chemical co.) and passed through a sieve with a mesh size of 30. A certain amount of sieved algae was soaked in $ZnCl_2$ solution with a specific ratio of 1 : 1 w/w. $ZnCl_2$ impregnated algae were homogenized by an ultrasonic apparatus at 60 °C for 30 min. The prepared algae were stirred and heated to form slurry mixture. The slurry was dried in an electric oven at 105 °C for 24 hours. The dried material was placed in an electric furnace with a heating rate of 5 °C min^{-1}, under nitrogen gas at 800 °C for 2 hours. Sufficient time was given to the prepared activated carbon for cooling in electric furnace and then the samples refluxed with diluted hydrochloric acid for 2 hours. The prepared activated carbon was rinsed with distilled water to reach a neutral pH. Eventually, this sample was dried at 110 °C for 12 hours and used for production of activated carbon-Fe_3O_4.

3. Synthesis of Fe_3O_4 Nanoparticles

Iron oxide nanoparticles were prepared by co-precipitation - chemical method. According to this method, an appropriate amount

Table 2. Range and levels of the variables for designing by the Box-Behnken

Factor	Unit	Coded symbol	Levels		
			Low (−1)	Central (0)	High (+1)
pH	-	A	3	6	9
Adsorbent dose	g/L	B	1	1.5	2
CEX concentration	mg/L	C	25	50	75
Contact time	min	D	30	60	90

of iron chloride (III) and iron chloride (II) (2 : 1 ratio) was homogenized in a three-headed balloon (contain 100 mL distilled water) under nitrogen gas inside the ultrasonic apparatus. During homogenization in an atmosphere of nitrogen gas, 20 mL of ammonia solution was added until the solution pH reached to around 9. A black deposit containing magnetite nanoparticles was formed at pH 9. The precipitate was homogenized for 45 min, then rinsed with distilled water to flush out impurities. Finally, using a 1.2 Tesla magnet, the magnetized Fe_3O_4 nanoparticles were separated and dried at 70 °C for 12 hours at the oven and stored in dark containers [30].

4. Production Magnetic Adsorbent of Activated Carbon-Fe_3O_4

The AC-Fe_3O_4 nanocomposite was synthesized according to a procedure reported in the literature [31]. Prepared activated carbon and Fe_3O_4 nanoparticles with the weight ratio of 10 : 1 were added to 200 mL of distilled water and homogenization was done at 70 °C for 15 min in an ultrasonic bath. The mixture was placed on the stirrer at 300 rpm for 2 hours to process the magnetic nanoparticle loading onto the activated carbon. The composite was rinsed with distilled water and then separated by a Tesla 1.3 magnet and then dried at 70 °C for 12 hours.

5. Characterization of the Adsorbent

Shape, morphological characteristics, and the size of the composite were analyzed by field emission scanning electron microscopy (FE-SEM). FE-SEM images of the samples were obtained on a MIRA3 TESCAN at an accelerating voltage of 30 kV. X-ray diffraction (XRD) analysis of the magnetic adsorbent was done with a Philips X-ray diffractometer (λ=1.5406 Å, 40 kV, 30 mA) in 2 theta range of 2-80° at a scanning rate of 1°/min. The magnetic properties of the adsorbent were evaluated using a vibrating sample magnetometer (VSM). The nitrogen adsorption/desorption isotherms were conducted by BET analysis (II BELSORP mini) at 77 K to determine the pore volume and specific surface area of the AC-Fe_3O_4 nanocomposite. Finally, for the characterization of functional groups, FT-IR spectra of the samples were taken using a Bruker-Tensor 27 model FT-IR spectrometer in the range of 450-4,000 cm^{-1}. For determination of pH at the point of zero charge (pH_{pzc}), 0.01 M NaCl was prepared and its pH was adjusted in the range of 2-12 by adding NaOH or H_2SO_4. 100 mL of NaCl (0.01 M) was added to the solutions and then 0.5 g/L of the AC-Fe_3O_4 nanocomposite added to these solutions. The flasks containing solutions were kept for 48 h, and the final pH of the solution was measured by using pH meter. Graphs were then plotted for pH_{final} vs. $pH_{initial}$.

6. Optimization of Adsorption Process by RSM Method

RSM based on the Box-Behnken was used to evaluate the effect of independent variables on the response function (CEX removal efficiency). Independent variables included pH, adsorbent dose, CEX concentration, and contact time at three levels (−1, 0, +1) as presented in Table 2. The number of experiments was calculated using the equation N=2K (K−1)+C, where N is the frequency of samples, K is the frequency of variables, and C is the frequency of central points, and a total of 27 tests were calculated for the experiments. The function of the response in general, which is a function of the encoded variables, is represented by the following quadratic polynomial equation:

$$Y=b_0+b_1A+b_2B+b_3C+b_{11}A^2+b_{22}B^2+b_{33}C^2+b_{12}AB+b_{13}AC+b_{23}BC+\varepsilon \quad (1)$$

The coefficients of the polynomial model are expressed as b_0 (constant expression) and b_1, b_2, b_3 (linear effects), b_{11}, b_{22}, b_{33} (second order effects) and b_{12}, b_{13}, b_{23} (interactive effects). The significance of each of the sentences in the regression equation was investigated, and significant expressions were identified in the model by Anova for each response. The R^2 and $R^2_{Adjusted}$ were used to determine the efficiency and validity of the model. The statistical model of Anova was used as a method for analyzing the responses.

CEX adsorption studies were performed on activated carbon regarding the effect of pH, the amount of adsorbent, CEX concentration, and reaction time. After completion of the reaction time, the samples were separated using a magnet and the residue of CEX in the solution was measured using a Lambda25 spectrophotometer apparatus, Perkin Elmer, at a maximum absorbance wavelength of 261 nm [32]. The efficiency of CEX removal (%) was calculated as [33-35].

$$\text{Cephalexin Removal (\%)} = \frac{C_o - C_e}{C_o} \times 100 \quad (2)$$

where C_o and C_e are the initial and equilibrium concentration of CEX in the solution (mg/L), respectively. Then adsorption capacity (q_e, mg/g) was calculated by the following mass balance relationship:

$$\text{Adsorption capacity, } q_e = \frac{(C_o - C_e) \times V}{M} \quad (3)$$

where q_e is the amount of CEX adsorbed per unit mass of the adsorbent (mg/g); V is the volume of the solution (L) and M is the adsorbent mass (g). Excel and design experiments software (Version 7) were used to analyze the results.

RESULTS AND DISCUSSION

1. Characterization of the Adsorbent

1-1. FTIR Analysis

The FTIR spectra of Fe_3O_4 and AC-Fe_3O_4 are shown in Fig. 1. In the FTIR spectra of Fe_3O_4 and AC-Fe_3O_4, the presence of Fe_3O_4

nanoparticles can be confirmed by the appearance of strong absorption bands at 583, 636, and 584 cm^{-1}. The broad and strong absorption peaks over 3,200-4,000 cm^{-1} and at 1,634 cm^{-1} are attributed to O-H stretching vibration and H-O-H bending vibration of H_2O absorbed by the Fe_3O_4 and AC-Fe_3O_4 nanocomposite, respectively. The other absorption bands can be attributed to the stretching vibration of C=C at 1,591 cm^{-1}, the stretching vibration of C-O at 980 and 916 cm^{-1} and stretching vibration of C-H at 870 cm^{-1} [36,37].

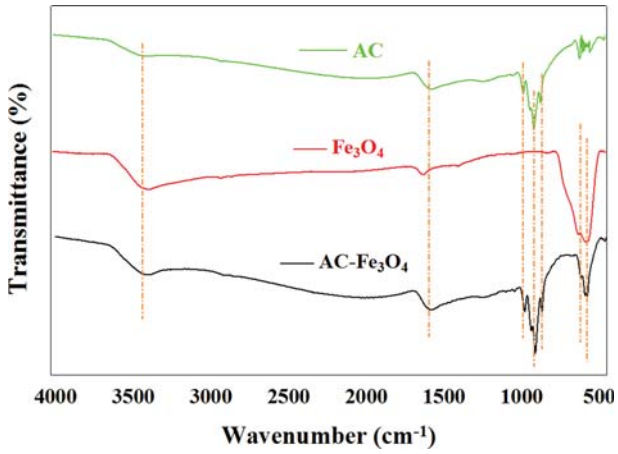

Fig. 1. FT-IR spectra of pure Fe_3O_4, AC and AC-Fe_3O_4 nanocomposite.

1-2. XRD Analysis

Fig. 2 illustrates the XRD patterns of the AC-Fe_3O_4 in the range of 2θ=10-80°. In the AC-Fe_3O_4, the characteristic diffraction peak at 28.8° is assigned to activated carbon. For Fe_3O_4, the peaks observed at 30.8°, 35.7°, 43.43°, 53.03°, 56.67° and 62.6° can be indexed

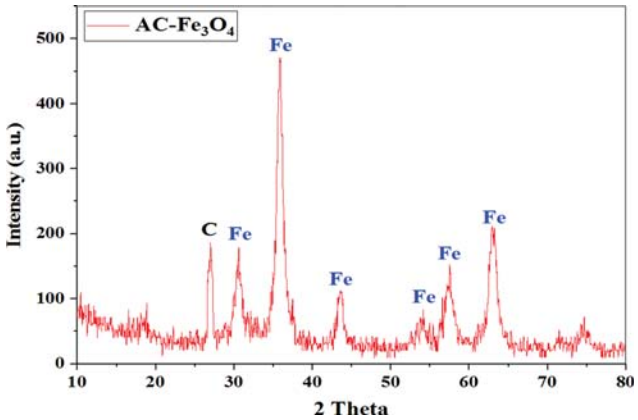

Fig. 2. XRD pattern of the AC-Fe_3O_4.

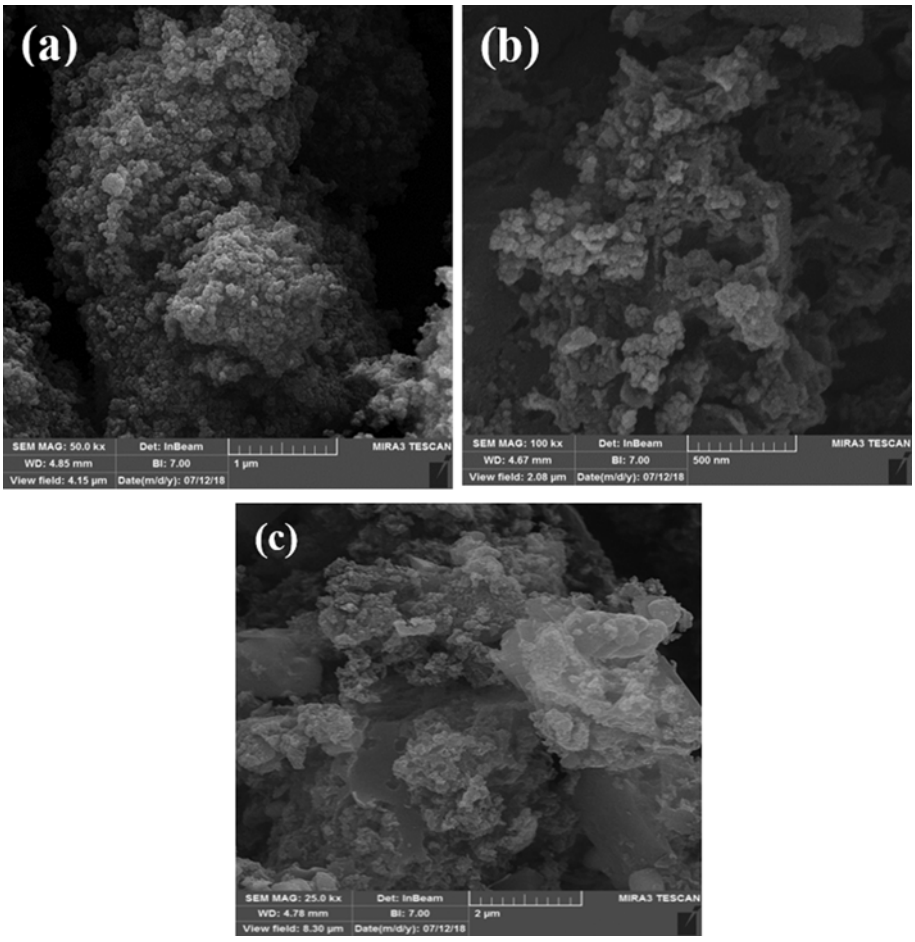

Fig. 3. FE-SEM images of (a) pure Fe_3O_4, (b) AC-Fe_3O_4 nanocomposite and (c) pristine AC.

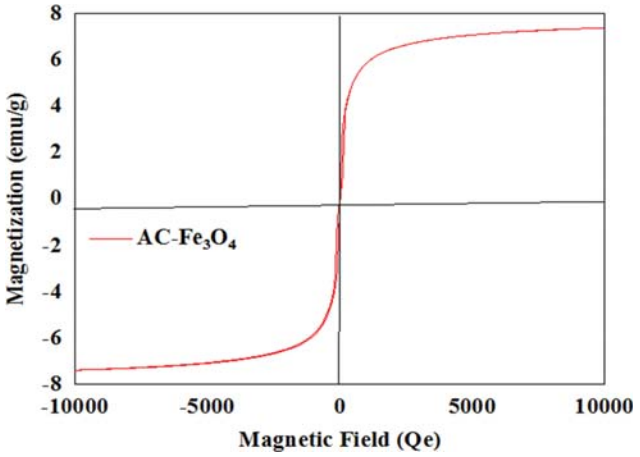

Fig. 4. Magnetization hysteresis loops at room temperature of the AC-Fe_3O_4.

Fig. 5. The separation of the AC-Fe_3O_4 from the solution: (a) is solution before separation of AC-Fe_3O_4, (b) solution after separation of AC-Fe_3O_4 and (c) external magnetic.

as the cubic inverse spinel structure of Fe_3O_4. The results of XRD analysis indicated that magnetic materials were synthesized and coated onto the activated carbon successfully.

1-3. FE-SEM Analysis

Fig. 3(a) clearly shows that nanoparticles were formed. The morphology of nanoparticles is spherical and a number of nanoparticles were stacked together and formed coarse particles. As seen in Fig. 3(b), activated carbon has a ripple surface and also has many pores that are clearly visible in Fig. 3. In Fig. 3(a) the diameter of Fe_3O_4 particles is in the range of 10-25 nm. As seen from Fig. 3(b), Fe_3O_4 nanoparticles are deposited in cluster form on the AC sidewalls. Pristine AC before modification is provided in Fig. 3(c) for better comparison. The FE-SEM analyses confirmed the formation of the AC-Fe_3O_4 nanocomposite [38].

1-4. VSM Analysis

Fig. 4 shows the VSM analysis for the synthesized composite at room temperature (25 °C) in the range of the magnetic field of ±10 (KOe) and at the saturation magnetization range of 8 ± emu/g. The results of this analysis show that the highest amount of saturation magnetization for the composite is 7.36 emu/g. As seen in Fig. 5, the composite has a significant magnetic property to be separated by magnets.

1-5. BET Analysis

Fig. 6(a) and (b) shows the nitrogen adsorption/desorption isotherms and pore size distribution of the AC-Fe_3O_4 nanocomposite and AC. The measurement of pore size distributions (PSDs) of adsorbents is based on the interpretation of gas adsorption measurements through adsorption equilibrium models. In this study, the specific surface areas (S_{BET}) and pore size distribution of adsor-

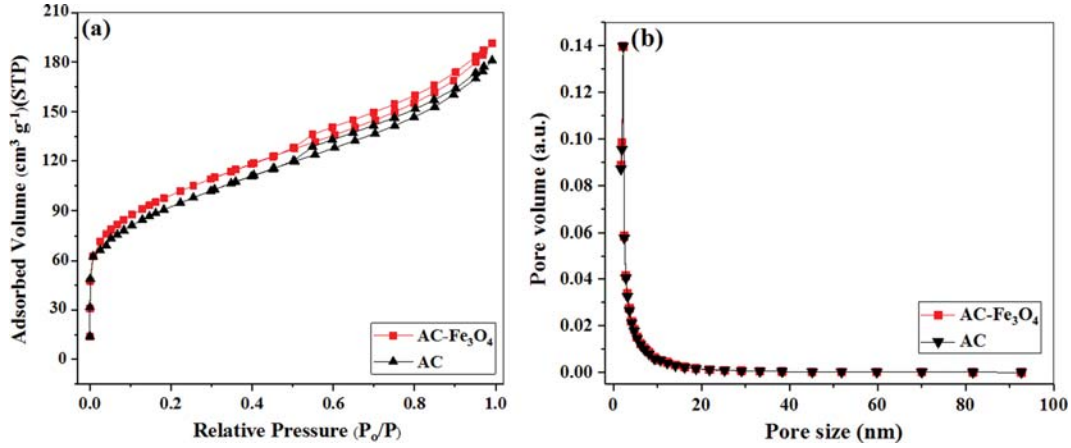

Fig. 6. (a) N_2 adsorption - desorption isotherm and (b) the pore size distribution.

Table 3. Specific surface area (S_{BET}), micropore specific surface area (S_{micro}), mesopore specific surface area (S_{meso}), total pore volume (V_{Total}), micropore volume (V_{micro}) and mesopore volume (V_{meso}) of AC and AC-Fe_3O_4

Material	S_{BET} (m^2/g)	S_{micro} (m^2/g)	S_{meso} (m^2/g)	V_{Total} (cm^3/g)	V_{micro} (cm^3/g)	V_{meso} (cm^3/g)	D_p (nm)
AC	149.56	86.65	62.91	0.3561	0.1224	0.2337	2.34
AC-Fe_3O_4	168.36	98.25	70.11	0.3899	0.1411	0.2488	2.34

bents were calculated by the multipoint Brunauer-Emmett-Teller (BET) and Barrett-Joyner-Halenda (BJH) methods. According to IUPAC classification, the isotherms can be classified as type-IV, which indicates that the AC-Fe_3O_4 nanocomposite and pristine AC are porous and mesoporous, respectively. As Fig. 5 shows, the AC-Fe_3O_4 nanocomposite has BET higher than the AC. The specific surface area (S_{BET}) and pore volume of adsorbents are compiled in Table 3. The AC-Fe_3O_4 nanocomposite and AC show an average pore diameter of 2.34 nm, which can allow ions to penetrate easier into their pores [39,40].

2. Analysis of the Central Composite Design

2-1. Response Surface Method

The response surface method investigates the relationship between the experimental and predicted results [41]. Box-Behnken design was used to achieve the most appropriate model for the optimization of the operational parameters at three levels. Box-Behnken matrix for the experimental and predicted results of the removal of CEX by the AC-Fe_3O_4 adsorbent is presented in Table 4. All experiments were designed to determine the optimal conditions and to investigate the effect of operating parameters on CEX removal. The predicted values were obtained by fitting the model with Design-Expert software, and the results indicate that the predicted values have a good correlation with the experimental values. Data fitting was performed using various models such as linear, quadratic, and cube models to obtain regression equations. As shown in Table 5, a quadratic model is the most suitable model for remov-

Table 4. Design matrix and levels based on the Box-Behnken

Run	pH	Concentration (mg/L)	Dose (g/L)	Time (min)	Removal actual (%)	Removal predicted (%)	Capacity adsorption (mg/g)
1	3	50	1	60	48.46	47.39	24.23
2	3	75	1.5	60	53.41	52.8	26.71
3	3	25	1.5	60	82.80	82.48	13.80
4	9	75	1.5	60	28.21	41.64	14.11
5	6	25	1.5	90	89.68	86.87	14.95
6	3	50	1.5	30	59.64	60.77	19.88
7	9	50	2	60	65.70	63.63	16.43
8	9	50	1.5	30	46.76	46.89	15.59
9	6	75	2	60	62.07	64.19	23.28
10	6	50	1	30	41.20	42.37	20.60
11	6	75	1.5	90	57.12	60.94	28.56
12	3	50	1.5	90	69.40	71.2	23.13
13	9	25	1.5	60	59.40	69.93	9.90
14	6	25	1.5	30	72.28	71.39	12.05
15	3	50	2	60	83.74	83.64	20.94
16	9	50	1.5	90	60.92	61.55	20.31
17	6	50	2	90	82.88	82.92	20.72
18	6	25	1	60	65.28	65.09	16.32
19	6	75	1.5	30	45.76	45.43	22.88
20	6	50	1	90	48.46	54.57	24.23
21	6	50	1.5	60	63.28	62.71	21.09
22	6	50	2	30	71.58	70.2	17.90
23	9	50	1	60	55.74	43.7	27.87
24	6	75	1	60	35.47	35	26.60
25	6	50	1.5	60	62.66	62.71	20.89
26	6	50	1.5	60	63.50	62.71	21.17
27	6	25	2	60	89.68	92.07	11.21

Table 5. Anova for the proposed model

Source	Sum of Squares	Df	Mean square	F value	P-value (Prob>F)	Remarks
Linear	223.31	20	11.17	19.26	0.0505	
2FI	141.01	14	10.07	17.37	0.0557	
Quadratic	56.66	10	5.67	9.77	0.0963	Suggested
Cubic	30.09	2	15.05	25.95	0.0371	Aliased
Pure error	1.16	2	0.58	-	-	

Table 6. Analysis of Anova for CEX removal using the AC-Fe_3O_4

Source	Degrees of freedom	Sum of squares	Mean square	F_o	P-value	Status
Model	14	5940.73	424.34	88.07	<0.0001	Significant
A	1	421.54	421.54	87.49	<0.0001	Significant
B	1	2366.58	2366.58	491.17	<0.0001	Significant
C	1	2520.20	2520.20	523.05	<0.0001	Significant
D	1	465.75	465.75	96.66	<0.0001	Significant
A.B	1	66.59	66.59	13.82	0.0029	Significant
A.C	1	0.47	0.47	0.098	0.7592	Not significant
A.D	1	4.84	4.84	1.00	0.3360	Not significant
B.C	1	1.21	1.21	0.25	0.6253	Not significant
B.D	1	0.068	0.068	0.014	0.9077	Not significant
C.D	1	9.12	9.12	1.89	0.1940	Not significant
A^2	1	40.29	40.29	8.36	0.0135	Significant
B^2	1	0.75	0.75	0.16	0.7002	Not significant
C^2	1	16.30	16.30	3.38	0.0908	Not significant
D^2	1	0.17	0.17	0.035	0.8542	Not significant
Residual	12	57.82	4.82			
Lake of fit	10	56.66	5.67	9.77	0.0963	Not significant
Pure error	2	1.16	0.58			
Core total	26	5998.55				

ing CEX by adsorption using the AC-Fe_3O_4 adsorbent (suggested model by software). The coefficients of R^2, adjusted R^2, and the fitting weakness are used for model validation. The closer R^2 value to 1 shows the power of the model fitness in describing response variations as a function of the independent variables [42]. According to Table 4, the regression coefficients, R^2, and adjusted R^2 represent a good fit model. The values of R^2 and adjusted R^2 are high, indicating that the model is statistically appropriate [43].

2-2. Quadratic Polynomial Model and Anova Analysis

Based on the Box-Behnken design, the empirical equation between input variables and experimental results is presented by a quadratic polynomial. The resulting equation based on encoded factors is:

$$Y=+62.71-5.93A+14.04-14.49+6.23D-4.08AB+0.34AC+1.1AD+0.55BC+0.13BD-1.51CD-2.75A^2-0.37B^2+1.75C^2+0.18D^2 \quad (4)$$

where Y is CEX removal (%) and A, B, C, and D are encoded variables that represent pH, adsorbent dose, initial CEX concentration, and reaction time, respectively. In addition, the accuracy of this quadratic model and determination of the most influential parameters in the CEX adsorption process were evaluated; the evaluation of the simultaneous effects of the operational parameters in the adsorption process was also evaluated by Anova. The results of the analysis of degrees of freedom (DF), the sum of squares (seq SS), mean square (adj MS), significant level (P-value) and Fisher test (F-Value) are shown in Table 6. The data obtained from Anova show that the proposed model has a statistically significant relationship with linear conditions according to one-way Anova ($p<0.001$).

According to Table 6, the effects of main operational parameters (reaction time, pH, the initial concentration of CEX, and adsorbent amount) on CEX removal are very significant ($P<0.001$), and the simultaneous interaction of some parameters (reaction time and pH) also has a significant effect on CEX removal ($P<0.001$). A significant level (P-value) plays the most crucial role in determining whether the interaction of variables is significant or not. Also, if the P-value is less than 0.001, the significance of the model and the variable is high [44]. The F-value parameter is a standard deviation of the mean value. The F value for this model was 88.08, which indicates that the variance of each variable is significant as compared to the error variance and the model is entirely significant. F-values indicated that the effect of different parameters on the process follows the following sequence: Initial concentration> adsorbent dose>reaction time>pH. The initial concentration with F=523.05 is the most effective factor in the removal of CEX with this adsorbent. R^2, adjusted R^2, and predictable coefficients for the model are presented in Table 7. The adjusted correlation coefficient (adjusted R^2) is equal to 0.9919 and the correlation coefficient, R^2, is equal to 0.9904 for adsorption of CEX, which is quite indicative of the high accuracy of the selected model. Difference between the adjusted R^2 and the predicted R^2 value should be less than 0.2, which in this study was less than 0.2.

Table 7. Correlation coefficients for the proposed quadratic model

Parameter	Value	Parameter	Value
Standard deviation	2.20	R-squared	0.9904
Mean	62.18	Adj R-squared	0.9791
C.V.%	3.53	Pred R-squared	0.9452
PRESS	328.97	Adeq precision	34.882

2-3. Examination of the Accuracy and Validity of the Proposed Model

Different analyses were carried out to investigate the validity of the proposed statistical model. Fig. 7(a) shows the experimental

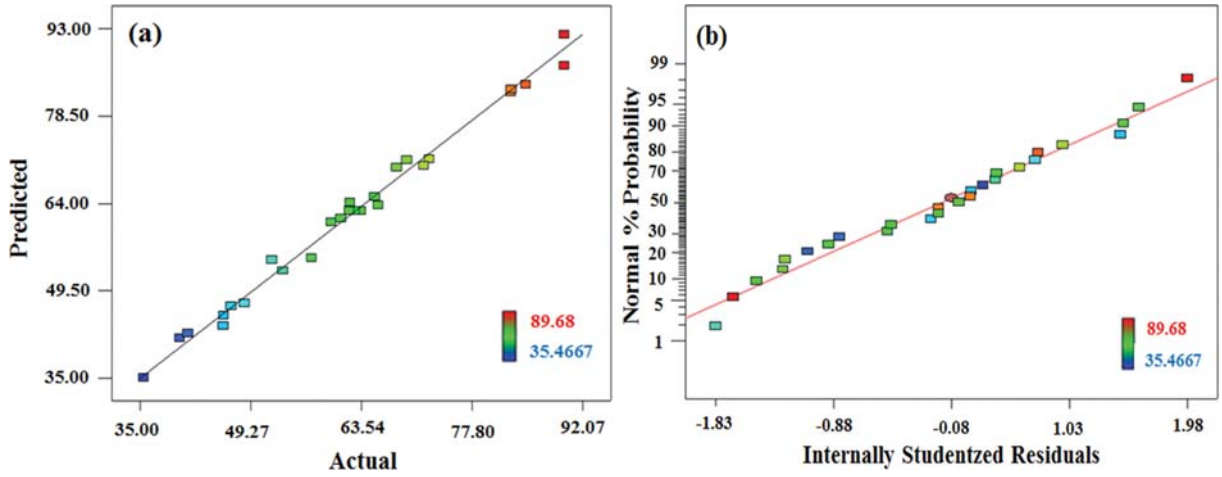

Fig. 7. (a) Experimental data versus predicted data by the statistical model and (b) normal probability and distribution.

data versus the predicted data by the statistical model that the values are uniformly distributed along a straight line and are highly correlated. Statistical analysis for verifying normal distribution of empirical data is necessary [45,46]. Fig. 7(b) shows a normal distribution of data and accordingly the data are very close together along the line.

2-4. Determination of Optimal Conditions for the Adsorption Process

Optimum conditions were determined to achieve the maximum removal of CEX using the AC-Fe_3O_4 adsorbent. Derringer's desirability function was used to determine the optimal value of independent variables. In the process mentioned above, the range of removal efficiency was examined in the range 0 to 1, where 0 indicates undesirable conditions, and the number 1 indicates the optimal operating conditions [47]. To optimize the process of adsorption, the main parameters including initial concentration of CEX (25, 50, and 75 mg/L), pH (3, 6, and 9), reaction time (30, 60, and 90 min), and adsorbent dose (1, 1.5, and 2 g/L) were investigated for maximum desirability. Fig. 8 shows that in optimal conditions (initial concentration of CEX 28.16 mg/L, the adsorbent dose of 2 g/L, pH of 3.02, and reaction time of 30.04 min), the CEX removal rate is

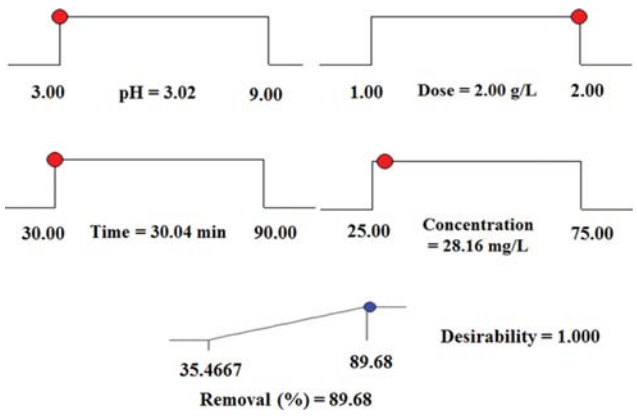

Fig. 8. The optimum conditions for adsorption of CEX using the AC-Fe_3O_4 adsorbent.

89.68%, which is in the desirability condition equal to 1.

3. Effect of Different Parameters on the Efficiency of CEX Removal

3-1. Effect of pH on the Efficiency of CEX Removal

The pH of the aqueous solutions plays an essential role in the adsorption process. Fig. 9(a) shows the effect of the pH and the initial concentration of CEX on adsorption process. Solution pH influences functional groups of CEX and the AC-Fe_3O_4. On the other hand, the adsorbent surface charge is influenced by the pH of the solution. According to Fig. 9(a), the removal efficiency increases by decreasing the pH from 9 to 3 and by decreasing the initial concentration of CEX from 75 to 25 mg/L. According to Fig. 9(d), the pH_{pzc} value in the AC-Fe_3O_4 nanocomposite was obtained at 7.38. The AC-Fe_3O_4 has a positive charge at pH<pH_{pzc} and has a negative charge at pH>pH_{pzc}. At lower pH values, the density of positive charges increases on the surface of the adsorbent, and therefore, the electrostatic attractive force increases between the positively charged adsorbent and CEX molecules. CEX has two functional groups of hydroxide with a pKa of 2.56 and the amine group with a pKa of 6.88 that is considered as an anionic molecule. Adsorption of CEX decreases with increasing pH value due to the increase of OH^- ions in the solution and the competition between hydroxide ions and CEX anions to reach the positive surface of the adsorbent. At higher values of pH, the number of sites at the surface of the adsorbent with negative charges increases and the number of the positively charged sites decreases, which results in an increase in repulsive force, which is not promising for adsorption of CEX. Legnoverde et al. [48] carried out a study to remove CEX using mesoporous silica and found that with increasing pH, the efficiency of antibiotic removal decreased [48]. In another study, Pouretedal and Sadegh [49] used grape wood to make activated carbon for the removal of CEX, tetracycline, amoxicillin, and penicillin from aqueous solutions. They found that the efficiency of the removal of antibiotics increased at acidic pH, which is in good agreement with our result [49].

3-2. Effect of Initial Concentration on the Efficiency of CEX Removal

Fig. 8(b) shows the initial concentration of CEX versus adsorbent

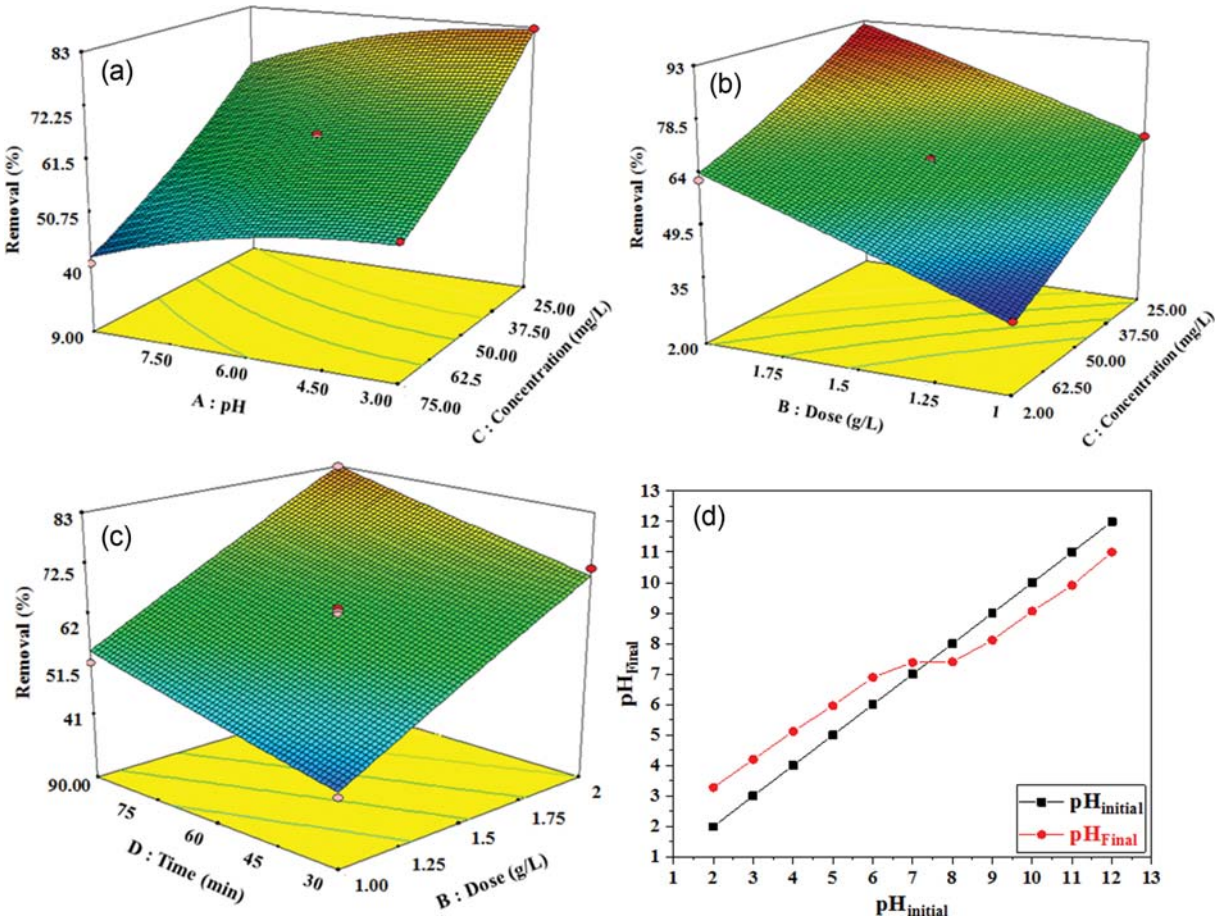

Fig. 9. Effect of pH at various initial concentrations on CEX (a), adsorbent dose and initial concentration of CEX (b) and adsorbent dose, contact time (c) and pH_{pzc} value (d).

dose in the adsorption process (three concentrations of 25, 50, and 75 mg/L). According to Fig. 8(b), with increasing the initial concentration from 25 mg/L to 75 mg/L, the efficiency of adsorption was reduced. In low concentrations of CEX, the availability of antibiotic molecules to active sites in the adsorbent surface is high, and as a result, CEX is adsorbed with higher efficiency on the surface of AC-Fe_3O_4. However, by increasing the CEX concentration in the solution, available active sites decrease. As a result, the adsorption efficiency showed a decreasing trend [50]. On the other hand, the adsorption capacity (q_e) increased with increasing the initial concentration of adsorbate. The reason for this phenomenon may be due to higher driving force in higher initial concentration of adsorbate [51]. Homem et al. used almond shell ash to remove amoxicillin from aqueous solution and found similar results [52]. Also, Miao et al. found a similar result in their study of removal of CEX with alligator weed [53].

3-3. Effect of the AC-Fe_3O_4 Adsorbent Dose on the Efficiency of CEX Removal

Fig. 8(c) shows the changes in the CEX adsorption process with variations in the adsorbent dose and reaction time. The results show that by increasing the adsorbent dose and reaction time, the CEX removal efficiency increases; however, the adsorbent dose has considerable influence on the CEX removal efficiency compared to reaction time. Increasing adsorption efficiency by increasing the adsorbent dose is due to the more available active sites and also the creation of a higher contact chance between the pollutant and the adsorbent. At lower doses, the adsorbent has fewer active sites for CEX molecules, reducing the removal efficiency. However, according to Eq. (3), with the increase of adsorbent dose the amount of adsorbed CEX per unit mass of adsorbent (q_e) decreases, because more sites on the adsorbent surface remain vacant. As shown in Fig. 8(c), with increasing reaction time, the chance of contact of CEX molecules with the adsorbent increased, and the amount of efficiency of CEX removal increased considerably at the beginning of the process and over time. The CEX removal rate decreases and eventually stays constant [54]. These results are consistent with the findings of Wu et al. who examined the removal of CEX using modified bio-char supported Ag/Fe nanoparticles [55]. Similar results were obtained by Babaei et al. on the removal of tetracycline with multi-walled carbon nanotubes adsorbent [13].

4. Equilibrium Study

The study of adsorption isotherms is important for optimizing the performance of wastewater treatment systems**.** In this study, Langmuir and Freundlich models were used to evaluate the interaction between CEX and the adsorbent. The linear form of the Langmuir isotherm model is given below [56]:

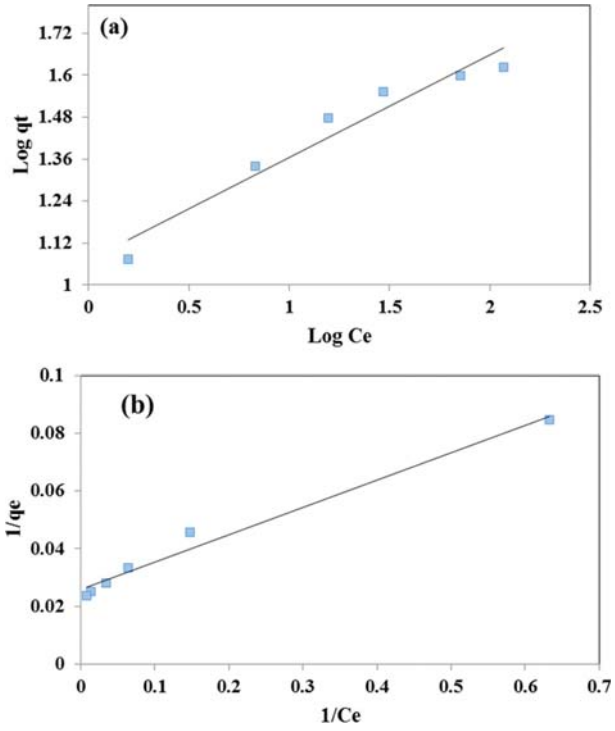

Fig. 10. Freundlich (a) and Langmuir (b) isotherms in adsorption of CEX.

$$\frac{1}{q_e}=\frac{1}{k_L q_m c_e}+\frac{1}{q_m} \quad (5)$$

where q_m represents the maximum adsorption capacity; k_L is the Langmuir constant that can be obtained from plotting $1/q_e$ versus $1/C_e$.

The Freundlich isotherm model assumes that adsorption takes place at a heterogeneous adsorbent surface, and the amount of adsorption depends on the equilibrium concentration of the adsorbate in the solution. According to this equation, by increasing the surface coating, the absorption energy is reduced logarithmically, due to the heterogeneity of the surface [57,58]. The Freundlich isotherm model is given below:

$$\log q_e=\log K_f+\frac{1}{n}\log c_e \quad (6)$$

where n and K_f indicate the adsorption intensity and the adsorption capacity, respectively, that can be calculated from the plot of log q_e versus log C_e. Isotherms equations were obtained at different concentrations of CEX (10, 25, 50, 75, 100, 150, and 200 mg/L) at the optimum pH of 3.02, adsorbent dose of 2 g/L and 45 min of equilibrium time.

In Fig. 10 and Table 8 the CEX adsorption onto AC-Fe_3O_4 follows the Langmuir isotherm model with a regression coefficient of 0.9803. According to Table 9, the q_{max} obtained from this study was found to be 38 mg/g. As provided in this table, q_{max} that resulted from the Langmuir isotherm in this study was compared with results of similar studies. q_{max} shows the adsorption capacity of adsorbate in mass unit of adsorbent. Higher value of q_{max} shows more capability of adsorbent to remove pollutants. As shown in Fig. 10(b), increasing the concentration leads to increased amount qe in the model. Experimental results showed that with increasing the CEX concentration from 25 to 200 mg/l, the amount of adsorbed CEX on adsorbate increased. The more concentration of CEX in fixed condition such as fixed dose of adsorbent results in increasing of driving force surrounding fixed mass of adsorbent and q_e will be higher. In addition, the value of R_L was between 0 and 1, which confirms that CEX adsorption by the AC-Fe_3O_4 is favorable. On the other hand, in the Freundlich model, the value of n is greater than 1, which indicates that the adsorption of CEX on the adsorbent is a favorable physical process. The results of the isotherm model of this study are consistent with the obtained results of other studies (in term of finding best model) that examined the removal of cephalexin from aqueous solution [53,59,60].

5. Study of Adsorption Kinetics

Kinetics models are used to determine process controlling factors, such as the speed of chemical reactions and the mass transfer mechanism. In the present study, the pseudo-first-order and pseudo-second-order kinetics were examined at different concentrations under optimum conditions at different times. In the pseudo-first kinetic, changes in the adsorption rate depend on the number of unoccupied sites at the adsorbent surface.

The linear form of the pseudo-first-order kinetic model is pre-

Table 8. The parameters of Langmuir and Freundlich models

Langmuir				Freundlich		
q_m (mg/g)	R^2	K_L	R_L	K_f [(mg/g) (mg/L)$^{1/n}$]	n	R^2
38.61	0.9803	0.272	0.127	11.74	3.39	0.9428

Table 9. Maximum sorption capacity of different adsorbents used for the adsorption of medical drugs

Adsorbent	pH	Concentration (mg/L)	q_{max} (mg/g)	Reference
AC from dende and babassu coconut	2-11	50	65-74	[51]
AC from bituminous coal (commercial)	2-10	10	34	[61]
AC (commercial) and biochar	3.5-10.5	1	20.6-37.5	[62]
AC from mung bean husk	2-12	100	26.5	[63]
AC-Fe_3O_4	3-11	30	38.61	This study

Table 10. Kinetics parameters of CEX adsorption under optimal conditions and different concentrations

		Pseudo-first-order			Pseudo-second-order		
C_O (mg/L)	$q_{e,exp}$ (mg/g)	$q_{1,cal}$ (mg/g)	k_1 (1/min)	R_1^2	$q_{2,cal}$ (mg/g)	k_2 (g/mg·min)	R_2^2
10	5.1	4.038	0.015	0.2779	5.05	2.94	1
25	12.55	4.90	0.022	0.8287	12.37	0.0026	0.998
50	23.85	11.64	0.023	0.8998	23.69	0.009	0.9976
75	30.4	18.08	0.027	0.9252	30.48	0.005	0.9955

sented by following equation [64]:

$$\log(q_e - q_t) = \log q_e - \left(\frac{k_1 t}{2.303}\right) \quad (7)$$

where q_t is the adsorption capacities at time t and k_1 is the constant coefficient of the pseudo-first-order kinetic.

The pseudo-second-order kinetic model is based on solid phase adsorption. q_e and k_2 are obtained by drawing a plot of t/q_e versus t. The linear form of the model is expressed in Eq. (9) [65]:

$$\frac{t}{q_e} = \frac{1}{(k_2 q_e^2)} + \left(\frac{1}{q_e}\right)t \quad (8)$$

where k_2 is the constant coefficient of the pseudo-second-order kinetic.

Regarding the kinetic constants and the correlation coefficients (R^2) presented in Table 10 and Fig. 11, as well as the comparison of experimental data with the calculated data, it can be stated that the kinetics of the adsorption follows the pseudo-second-order model. The results show that there are remarkable differences between the calculated adsorption capacity compared to the real data in the pseudo-first kinetic, but in the pseudo-second-order kinetic, this difference is negligible, which indicates that the data are fitted to the pseudo-second-order kinetic. In addition, the pseudo-second-order kinetic model has the highest correlation coefficient, so this kinetic model was considered as the best-fitted kinetic model. Al-Khalisy et al. [19] showed that adsorption of CEX from aqueous solutions by bentonite and activated carbon followed the pseudo-second-order kinetic model [19].

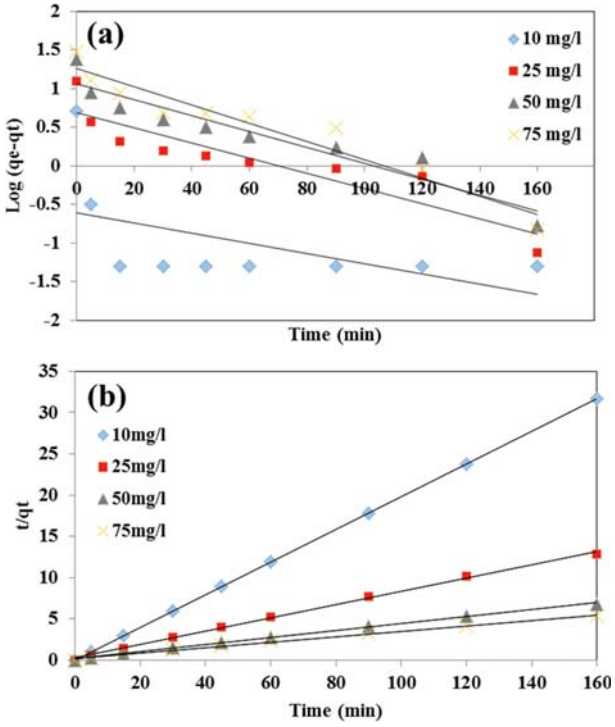

Fig. 11. Pseudo-first-order kinetic (a) and pseudo-second-order kinetic (b) for the adsorption of CEX.

6. Reusability of the Adsorbent

Regeneration of AC-Fe_3O_4 nanocomposite was studied using by washing and drying (at 105 °C) process for adsorption of CEX. The recovered samples after washing with distilled water and then drying were examined in optimum condition again for studying removal efficiency of CEX by regenerated adsorbent. As shown in Fig. 12, the generation process was carried out for five times. Generally, the nanocomposite capacity for removal of CEX was reduced with increasing number of regeneration cycles. The value of removal efficiency by regenerated adsorbent was 87.68% for the first regeneration. The trend of regenerations shows that the decrease in removal efficiency was relatively clear, and after the fifth cycle, the absorption capacity decreased to 47.6%. The results of regenerations showed that this nanocomposite has promising performance in primary steps for removal of CEX; however, the performance was reduced almost half after five cycles in regenerated conditions.

7. Effect of Cation and Anions

In this study, the effects of cation (Li^{+1}, K^{+1}, Mg^{+2}, Ca^{+2}, Ni^{+2} and

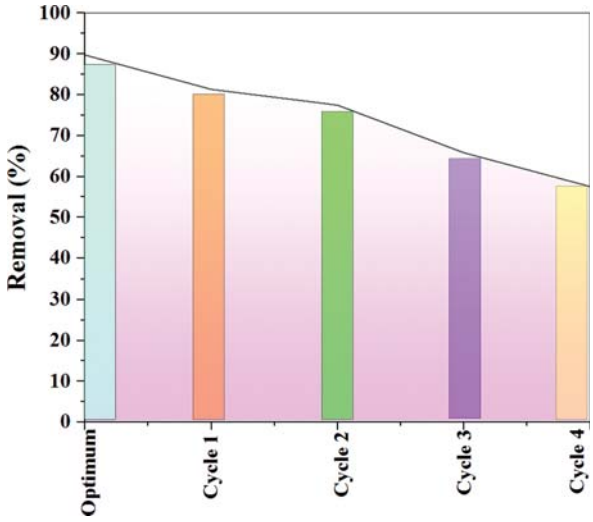

Fig. 12. Regeneration of adsorbent AC-Fe_3O_4 in four cycles.

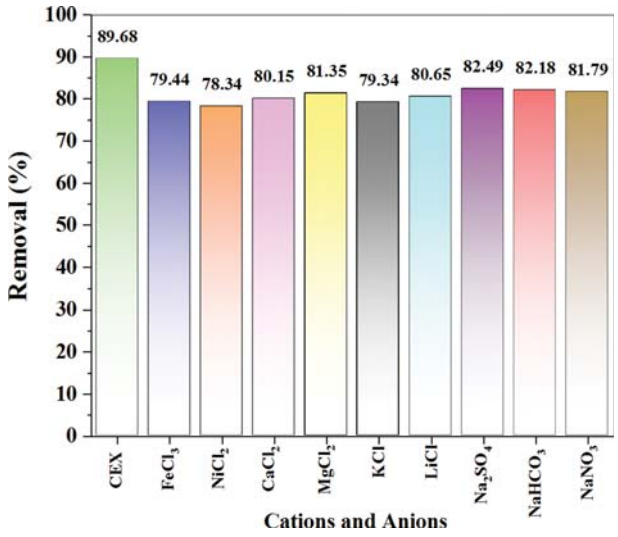

Fig. 13. The adsorption of CEX onto the AC-Fe_3O_4 in the presence of 1 mM cations and anions.

Fe^{+3}), and anions (SO^{-2}, NO^{-3}, HCO_3^{-1}) were examined that can interfere with the adsorption of CEX on AC-Fe_3O_4. The results of the experiments are shown in Fig. 13. As reported in previous papers, the concentration of anions and cation in surface waters is usually less than 1 mM; therefore, 1 mM of above mentioned anions and cation was examined to evaluate its effects on CEX adsorption. One of the reasons for the decrease in the adsorption of CEX in the presence of anions and cation can be a competition between ions and CEX molecule for adsorption at active sites of adsorbents. The results showed that Ni^{+2}, K^{+1} and Fe^{+3} had highest interference for adsorption of cefalexin on AC-Fe_3O_4. According to the result the removal efficiency decreases from 89.68 to 78.34 for presence of Ni^{+2}, from 89.68 to 79.34 for presence of K^{+1} and from 89.68 to 79.44 for presence of Fe^{+3}. The reduced percentage removal of cefalexin due to the presence of other anions and cations was found to be less than 10%. The reason for a higher reduction in removal efficiency in the presence of mentioned cations can be due to the tendency of these ions to adhere to active adsorbent sites in competition of cefalexin.

Other studies have reported the most reduction of adsorption efficiency in the presence of Ni^{+2}, K^{+1} and Fe^{+3} ions. Takdastan et al. studied the adsorption efficiency of activated carbon for removal of tetracycline antibiotic and reported that the removal efficiency decreases significantly in the presence of Ni^{+2} and Fe^{+3} [17]. Zhao et al. studied the removal of tetracycline by goethite in the presence cations and humic acid. They reported that the presence of some ions such as Li^{+1}, Na^{+1}, K^{+1}, Ca^{+2}, and Mg^{+2} had little effect on removal efficiency [66]. Results of this study showed that cations compared have more effect on adsorption of antibiotic on AC-Fe_3O_4. The removal of CEX was also studied in real wastewater media.

8. Real Wastewater Study

Actual wastewater containing antibiotics has many impurities that may interfere with the adsorption process. The results of removal efficiency of CEX were found to be 66.43% and 89.68%, in real and synthetic wastewater by AC-Fe_3O_4 nanocomposite, respectively. As expected, the removal amount is lower in real wastewater compared to synthetic wastewater. This efficiency decrease might be attributable to different pH ranges and the presence of organic materials and ions in real wastewater [67]. Additional costs may be required to remove some impurities before the absorption process.

CONCLUSION

AC-Fe_3O_4 nanocomposite was prepared by filamentous algae. Results showed the remarkable efficiency of the AC-Fe_3O_4 nanocomposite for the adsorption of CEX from aqueous solutions. The Box-Behnken model was used to study the effective parameters of the process separately and simultaneously. The increase in contact time and the amount of adsorbent makes increases in the process efficiency and, in contrast, the increase in pH and initial concentration of CEX reduces the adsorption efficiency. The fittest weakness model showed that the proposed model (quadratic) is quite promising for the adsorption of CEX on the AC-Fe_3O_4. Under optimal conditions (initial concentration of CEX 28.16 mg/L, the adsorbent dose of 2 g/l, the reaction time of 30.04, and pH=3.02), the process efficiency was 89.68% with a desirability level of 1. Equilibrium and kinetic studies indicated that the adsorption was fitted with Langmuir isotherm and kinetic model of pseudo-second-order. In addition, the regeneration of the AC-Fe_3O_4 nanocomposite showed that this adsorbent has promising capacity in five regeneration cycles for removal of CEX. The effect of cations and anion showed the decreasing effects on antibiotic removal efficiency. Due to high adsorption capacities and reusability, AC-Fe_3O_4 nanocomposite has a high potential for use in the treatment process for aqueous solution containing various pharmaceutical contaminants.

ACKNOWLEDGEMENTS

The authors would like to acknowledge Ardabil University of Medical Sciences for financial and instrumental supports (code: IR.ARUMS.REC.1397.178).

REFERENCES

1. J. Rivas, O. Gimeno and F. Beltrán, *Chemosphere*, **74**, 854 (2009).
2. B. Merzouk, K. Madani and A. Sekki, *Desalination*, **250**, 573 (2010).
3. Z. Fang, J. Chen, X. Qiu, X. Qiu, W. Cheng and L. Zhu, *Desalination*, **268**, 60 (2011).
4. M. Rakhshani, F. Rakhshani and A. Mirshahi, *KAUMS Journal* (FEYZ), **6**, 45 (2002).
5. M. Azadbakht, S. M. Mirjani, M. Yousofi and M. Amini, *J. Mazandaran Univ. Med. Sci.*, **24**, 44 (2015).
6. R. Kafaei, F. Papari, M. Seyedabadi, S. Sahebi, R. Tahmasebi and M. Ahmadi, *Sci. Total Environ.*, **627**, 703 (2018).
7. D. W. Kolpin, E. T. Furlong, M. T. Meyer, E. M. Thurman, S. D. Zaugg and L. B. Barber, *Environ. Sci. Technol.*, **36**, 1202 (2002).
8. K. Lata, R. Sharma, L. Naik, Y. Rajput and B. Mann, *Food Chem.*, **184**, 176 (2015).
9. L. Lloret, G. Eibes, T. Lú-Chau, M. Moreira, G. Feijoo and J. Lema, *Biochem. Eng. J.*, **51**, 124 (2010).
10. C. Bellona, J. E. Drewes, P. Xu and G. Amy, *Water Res.*, **38**, 2795

(2004).
11. M. M. Huber, S. Canonica, G.-Y. Park and U. Von Gunten, *Environ. Sci. Technol.*, **37**, 1016 (2003).
12. Y. Rashtbari, S. Hazrati, S. Afshin, M. Fazlzadeh and M. Vosoughi, *Data in Brief*, **20**, 1434 (2018).
13. A. A. Babaei, E. C. Lima, A. Takdastan, N. Alavi, G. Goudarzi and M. Vosoughi, *Water Sci. Technol.*, **74**, 1202 (2016).
14. D. Vogna, R. Marotta, A. Napolitano and M. d'Ischia, *J. Org. Chem.*, **67**, 6143 (2002).
15. O. Legrini, E. Oliveros and A. Braun, *Chem. Rev.*, **93**, 671 (1993).
16. G. Amy, T.-U. Kim, J. Yoon, C. Bellona, J. Drewes and J. Pellegrino, *Water Sci. Technol. Water Supply*, **5**, 25 (2005).
17. A. Takdastan, A. H. Mahvi, E. C. Lima, M. Shirmardi, A. A. Babaei and G. Goudarzi, *Water Sci. Technol.*, **74**, 2349 (2016).
18. S.-H. Lin and R.-S. Juang, *J. Environ. Manage.*, **90**, 1336 (2009).
19. R. S. Al-Khalisy, A. M. A. Al-Haidary and A. H. Al-Dujaili, *Sep. Sci. Technol.*, **45**, 1286 (2010).
20. Y. Zhang, W. Yan, Z. Sun, C. Pan, X. Mi and G. Zhao, *Carbohydr. Polym.*, **117**, 657 (2015).
21. A. Takdastan, A. H. Mahvi, E. C. Lima, M. Shirmardi, A. A. Babaei and G. Goudarzi, *A J. of the Int. Association on Water Pollut. Res.*, **74**, 2349 (2016).
22. H. Zhang, X. Li, G. He, J. Zhan and D. Liu, *Ind. Eng. Chem. Res.*, **52**, 16902 (2013).
23. V. Gupta and A. Nayak, *Chem. Eng. J.*, **180**, 81 (2012).
24. G. Absalan, A. Bananejad and M. Ghaemi, *Anal. Bioanalytical Chem. Res.*, **4**, 65 (2017).
25. S. Saber-Samandari, S. Saber-Samandari, H. Joneidi-Yekta and M. Mohseni, *Chem. Eng. J.*, **308**, 1133 (2017).
26. J. Zhang, B. Li, W. Yang and J. Liu, *Ind. Eng. Chem. Res.*, **53**, 10629 (2014).
27. M. A. Bezerra, R. E. Santelli, E. P. Oliveira, L. S. Villar and L. A. Escaleira, *Talanta*, **76**, 965 (2008).
28. J. Zolgharnein, A. Shahmoradi and J. B. Ghasemi, *J. Chemometrics*, **27**, 12 (2013).
29. H. Liu, W. Liu, J. Zhang, C. Zhang, L. Ren and Y. Li, *J. Hazard. Mater.*, **185**, 1528 (2011).
30. Z. Yang, L. Li, C. Hsieh and R. Juang, *J. Taiwan Inst. Chem. Eng.*, **82**, 56 (2018).
31. Y. Zhi-Feng, L. Ling-Yun, H. Chien-Te and J. Ruey-Shin, *J. Taiwan Inst. Chem. Eng.*, **82**, 56 (2018).
32. A. Mohseni-Bandpi, T. J. Al-Musawi, E. Ghahramani, M. Zarrabi, S. Mohebi and S. A. Vahed, *J. Mol. Liq.*, **218**, 615 (2016).
33. K. Nadafi, M. Vosoughi, A. Asadi, M. O. Borna and M. Shirmardi, *J. Water Chem. Technol.*, **36**, 125 (2014).
34. M. Haghighi, F. Rahmani, R. Dehghani, A. M. Tehrani and M. B. Miranzadeh, *Desalin. Water Treat*, **58**, 168 (2017).
35. S. Afshin, S. A. Mokhtari, M. Vosoughi, H. Sadeghi and Y. Rashtbari, *Data In Brief*, **21**, 1008 (2018).
36. D. Bhatia, D. Datta, A. Joshi, S. Gupta and Y. Gote, *J. Chem. Eng. Data*, **63**, 436 (2018).
37. A. Yaumi, M. A. Bakar and B. Hameed, *Energy*, **155**, 46 (2018).
38. Z.-F. Yang, L.-Y. Li, C.-T. Hsieh and R.-S. Juang, *J. Taiwan Inst. Chem. Eng.*, **82**, 56 (2018).
39. T. L. Silva, A. L. Cazetta, P. S. Souza, T. Zhang, T. Asefa and V. C. Almeida, *J. Cleaner Prod*, **171**, 482 (2018).
40. L. Khezami, A. Chetouani, B. Taouk and R. Capart, *Powder Technol.*, **157**, 48 (2005).
41. G. J. Swamy, A. Sangamithra and V. Chandrasekar, *Dyes Pigm.*, **111**, 64 (2014).
42. E. Jahed, M. Khodaparast, K. Behzad, M. Elahi and A. Koocheki, *Iranian Food Sci. Technol. Res. J.*, **8**, 60 (2012).
43. E. Jahed, M. H. H. Khodaparast and A. M. Khaneghah, *Appl. Clay Sci.*, **102**, 155 (2014).
44. K. Ravikumar, S. Ramalingam, S. Krishnan and K. Balu, *Dyes Pigm.*, **70**(1), 18 (2006).
45. V. Ponnusami, V. Krithika, R. Madhuram and S. Srivastava, *J. Hazard. Mater.*, **142**, 397 (2007).
46. M. R. Espejo, *Technometrics*, **48**(2), 304 (2006).
47. D. Awotwe-Otoo, C. Agarabi, P. J. Faustino, M. J. Habib, S. Lee and M. A. Khan, *J. Pharm. Biomed. Anal.*, **62**, 61 (2012).
48. M. S. Legnoverde, S. Simonetti and E. I. Basaldella, *Appl. Surf. Sci.*, **300**, 37 (2014).
49. H. R. Pouretedal and N. Sadegh, *J. Water Process Eng.*, **1**, 64 (2014).
50. M. R. Samarghandi, T. J. Al-Musawi, A. Mohseni-Bandpi and M. Zarrabi, *J. Mol. Liq.*, **211**, 431 (2015).
51. R. Ferreira, H. De Lima, A. Cândido, O. C. Junior, P. Arroyo and K. De Carvalho, *Int. J. Biol. Biomol. Agric Food Biotechnol. Eng.*, **9**, 717 (2015).
52. V. Homem, A. Alves and L. Santos, *Int. J. Environ. Anal. Chem.*, **90**, 1063 (2010).
53. M.-S. Miao, Q. Liu, L. Shu, Z. Wang, Y.-Z. Liu and Q. Kong, *Process Saf. Environ.*, **104**, 481 (2016).
54. A. B. Leite, C. Saucier, E. C. Lima, G. S. dos Reis, C. S. Umpierres and B. L. Mello, *Environ. Sci. Pollut. Res.*, **25**, 7647 (2018).
55. H. Wu, Q. Feng, H. Yang, E. Alam, B. Gao and D. Gu, *Colloids Surf., A*, **517**, 63 (2017).
56. H. Golestanifar, A. Asadi, A. Alinezhad, B. Haybati and M. Vosoughi, *Desalin. Water Treat*, **57**, 5480 (2016).
57. M. V. Niri, A. H. Mahvi, M. Alimohammadi, M. Shirmardi, H. Golastanifar and M. J. Mohammadi, *J. Water Health*, **13**, 394 (2015).
58. S. Afshina, Y. Rashtbaria, M. Shirmardic, M. Vosoughib and A. Hamzehzadeha, *Desalin. Water Treat*, **161**, 365 (2019).
59. M. J. Ahmed and S. K. Theydan, *Chem. Eng. J.*, **211**, 200 (2012).
60. M. Alipour, M. Vosoughi, S. A. Mokhtari, H. Sadeghi, Y. Rashtbari and M. Shirmardi, *Int. J. Environ. Anal. Chem.*, **1**, 232 (2019).
61. P. Iovino, S. Canzano, S. Capasso, A. Erto and D. Musmarra, *Chem. Eng. J.*, **277**, 360 (2015).
62. E. Kim, C. Jung, J. Han, N. Her, C. M. Park and A. Son, *Desalin. Water Treat*, **57**, 27601 (2016).
63. S. Mondal, K. Sinha, K. Aikat and G. Halder, *J. Environ. Chem. Eng.*, **3**, 187 (2015).
64. M. O. Borna, M. Pirsaheb, M. V. Niri, R. K. Mashizie, B. Kakavandi and M. R. Zare, *J. Taiwan Inst. Chem. Eng.*, **68**, 80 (2016).
65. H. Biglari, S. RodríguezíCouto, Y. O. Khaniabadi, H. Nourmoradi, M. Khoshgoftar and A. Amrane, *Int. J. Chem. Reactor Eng.*, **16**, (2018).
66. Y. Zhao, X. Gu, S. Gao, J. Geng and X. Wang, *Geoderma*, **183**, 12 (2012).
67. C. Zhang, C. Lai, G. Zeng, D. Huang, C. Yang and Y. Wang, *Water Res.*, **95**, 103 (2016).